

Formation of mesic nuclei by (γ, p) reactions

H. Nagahiro^a, D. Jido^{b 1} and S. Hirenzaki^c

^a*Research Center for Nuclear Physics (RCNP), Osaka University, Ibaraki, Osaka 567-0047, Japan*

^b*Physik-Department, Technische Universität München, D-85747 Garching, Germany*

^c*Department of Physics, Nara Women's University, Nara 630-8506, Japan*

Abstract

We present a theoretical study on formation rates of η and ω meson-nucleus systems induced by (γ, p) reactions on nuclear targets at ideal recoilless condition. We find that the smaller distortion effect in the (γ, p) reaction enables us to investigate properties of the mesons created deeply inside nucleus more clearly. We also consider excitation of scalar-isoscalar (σ) mode in nucleus in order to investigate spectral enhancement around two-pion threshold caused by partial restoration of chiral symmetry. We conclude that valuable information of meson-nucleus interactions can be extracted from global structure of the missing mass spectra in the (γ, p) reaction.

1 Introduction

The study of the in-medium properties of hadrons is one of the most important subjects in contemporary nuclear physics and has attracted continuous attention. The detailed investigation of hadron-nucleus bound systems clarifies quantitative information on basic hadron-nucleus interactions. This is one of the important steps for understanding the QCD phase structure. So far, atomic states of pion, kaon and \bar{p} have been investigated comprehensively and observed experimentally [1]. The recent interest reaches the extension to the systems with other heavier neutral mesons, such as the η and ω mesons, governed purely by strong interaction in contrast to the atomic states. The scalar-isoscalar (σ) excited mode in nucleus is also considered as one of the interesting systems.

¹Present address: Yukawa Institute for Theoretical Physics, Kyoto University, Kyoto 606-8502, Japan

Recent development in experimental aspect is the establishment of the $(d, {}^3\text{He})$ spectroscopies in the formation of the deeply bound pionic atoms [2–5]. It opens new possibilities of the formations of other hadron-nucleus bound systems [6–9]. The (γ, p) reaction is another experimental tool for formation of the hadron-nucleus system and originally proposed in Refs. [10–13]. The (γ, p) reaction, as well as the $(d, {}^3\text{He})$ reaction, is able to satisfy recoilless condition at the meson creation energy. The use of the (γ, p) reaction has good advantage that the distortion effects of the projectile and the ejectile are expected to be smaller than in the $(d, {}^3\text{He})$ reaction mainly due to the incident photon.

It is also important mentioning that, in the theoretical point of view, the study of the hadron in finite density gives us information on the QCD phase structure [14], such as partial restoration of chiral symmetry, in which a reduction of the chiral condensate takes place in nuclear density. In this line hadronic bound systems have been investigated in various chiral models [6, 7, 15–20].

In this paper, motivated by the successful study of the $(d, {}^3\text{He})$ reaction and the advantage of the smaller distortion effect, we discuss the (γ, p) reaction for studying the formations of the various meson-nucleus systems (η , ω and scalar-isoscalar (σ) mode) at the recoilless kinematics. Structure of the mesic nucleus is studied theoretically using the appropriate meson-nucleus optical potentials in nuclear matter. In order to evaluate the formation rates of the mesic nuclei, we introduce a Green function constructed by the Klein-Gordon equation with the optical potential, and calculate the cross section of the (γ, p) reaction on a nuclear target following the method by Morimatsu and Yazaki [21]. In the case of the scalar-isoscalar (σ) mode, we evaluate an effective spectral function of this mode in nucleus because of both the lack of the elementary cross section and the large imaginary part of sigma meson self-energy in vacuum, which requires certain modifications in the Green function method.

In the previous paper [6, 7] for studying the η -nucleus system in the chiral doublet model, we found repulsive nature of the η optical potential inside the nucleus which is associated with reduction of the mass difference of N and $N(1535)$ caused by partial restoration of chiral symmetry. Consequently there exist certain discrepancies between the spectra obtained by the chiral doublet model and the chiral unitary model. The discrepancies are expected to be distinguished by

experimental data [7]. However, in the $(d, {}^3\text{He})$ reaction, due to the large distortion effect, it might be difficult to obtain clear information about the optical potential in the nuclear center. Therefore, it is interesting to consider the (γ, p) reaction with much smaller distortion effects to explore the behavior of the η meson in the nucleus.

As another meson-nucleus systems, we consider the ω -mesic nuclei. The ω mesic nuclei were studied by several groups and the theoretical results have been reported in Refs. [8,9,12,16,17]. Recently, several experimental results have been also reported in Refs. [22,23]. Especially, in Refs. [12,16,17], one finds the ω self-energy in nuclear medium based on an effective model and the calculated (γ, p) spectra for the production of the ω -mesic nuclei at the recoilless kinematics. In the present paper, we calculate the (γ, p) spectra for the formation of the ω -mesic nuclei, and we show the incident γ energy dependence of the whole spectra and the dominant subcomponents to study the experimental feasibilities in the lower energy photon facilities. This study is also interesting for the higher energy photon facility like SPring-8, since the incident photon energy has a certain distribution and we need to use the photon with various energies around the ideal recoilless kinematics to get better statistics [24]. We also study the sensitivity of the expected spectra to the ω -nucleus interaction using another theoretical prediction [25].

We also consider the (γ, p) reactions in the scalar-isoscalar (σ) channel inspired by Ref. [26–28], where an enhanced spectral function near the 2π threshold has been pointed out as a characteristic signal of the partial restoration of chiral symmetry. This is associated with a conceivable reduction of the sigma mass and width in medium. Therefore, there might be a chance to create the σ mesic nuclei with relatively small widths, if deeply bound states are formed in heavy nuclei [18]. It has been also found difficult, in the (d, t) or $(d, {}^3\text{He})$ reactions, to observe the enhancement near the 2π threshold due to the large distortion effects [18]. In this paper, we explore the possibility of production of the σ -mesic nuclei by the photon-induced reactions, expecting that the ‘transparency’ of the (γ, p) reactions enables us to observe the enhancement of the spectral function near the 2π threshold caused by the partial restoration of chiral symmetry in the medium.

This paper is organized as follows. In Sec.2, we will discuss our model for the optical potential of each meson separately, and study

the structure of the mesic nuclei showing the binding energies and the widths obtained with the optical potential. In Sec.3, we will show the advantages of the (γ, p) reaction for the formation of the meson-nucleus system, and review briefly the formulation to calculate the formation spectrum of the mesic nucleus. In Sec.4, we will present the numerical results of the missing mass spectra of the (γ, p) reaction, and compare them with those of the $(d, ^3\text{He})$ reaction. Finally Sec.5 is devoted to summary of this paper.

2 Structure of mesic nuclei

In this section, we describe the theoretical formulation to study the structure of the meson-nucleus systems and show their numerical results, such as the binding energies and widths, within an optical potential approach, in which all the meson-nucleus interactions are summarized in an optical potential of the meson in nuclear matter.

The wave functions, the binding energies and their widths for the in-medium meson (if it is bound) are calculated by solving the Klein-Gordon equation with the optical potential. The Klein-Gordon equation is written as

$$\left[-\nabla^2 + \mu^2 + 2\mu V(\omega, \rho(r))\right] \phi(r) = E^2 \phi(r), \quad (1)$$

where μ denotes the meson-nucleus reduced mass, which is very close to the meson mass for heavy nuclei, ω is the real part of the relativistic meson energy E , and $V(\omega, \rho(r))$ presents the optical potential for the meson-nucleus system. Here we assume to neglect the momentum dependence of the optical potential, since we consider the recoilless condition on the (γ, p) reaction for the mesic nuclei formation, in which the meson will be created in the nucleus nearly at rest. The optical potential V and the eigenenergy E are expressed as complex numbers in general because of the absorptive effects of the nucleus. We need to solve the Klein-Gordon equation (1) in a self-consistent manner for the energy in case the optical potential V has the energy dependence. We follow the method of Kwon and Tabakin to solve the Klein-Gordon equation [29], which was successfully applied to calculate pionic atom states [30]. Here, we increase the number of mesh points in the momentum space about 10 times larger than the original work Ref. [29] as discussed in Ref. [6].

In the following parts of the present section, we discuss the in-medium optical potential $V(\omega, \rho)$ for the η , ω and σ mesons separately. We show the bound state spectra, if the mesons are bound, solving the Klein-Gordon equation (1) with the optical potential. Here we assume the local density approximation with the nuclear density distribution $\rho(r)$ written as the empirical Woods-Saxon form:

$$\rho(r) = \frac{\rho_0}{1 + \exp(\frac{r-R}{a})}, \quad (2)$$

with the radius of nucleus $R = 1.18A^{1/3} - 0.48$ fm and the diffuseness $a = 0.5$ fm for the nuclear mass number A .

2.1 η -nucleus optical potential

First of all, we discuss the η -nucleus system. The η -mesic nuclei were studied by Haider and Liu [31] and by Chiang, Oset and Liu [32]. As for the formation reaction, the attempt to find the bound states by the (π^+, p) reaction led to a negative result [33]. Recently, some experiments in photoproduction processes indicated observations of such bound states in ^{12}C target [34] and ^3He target [35], and another experiment is now planned to investigate the η -nucleus interaction [9]. In this study we use the same theoretical models for η -nucleus interaction as described in Refs. [6, 7] in further detail. In the η -nucleon system, the $N(1535)$ resonance (N^*) plays an important role due to the dominant ηNN^* coupling. Here we evaluate the η -nucleus optical potential $V_\eta(\omega, \rho(r))$ in the two different models which are based on distinct physical pictures of N^* . One is the chiral doublet model. This is an extension of the linear sigma model for the nucleon and its chiral partner [36–38]. The other is the chiral unitary model, in which N^* is dynamically generated in the coupled channel meson-baryon scattering [15, 39].

In the first approach, the N^* is introduced as a particle with a large width and appears in an effective Lagrangian together with the nucleon field. Assuming N^* -hole excitation induced by the η meson in nucleus, we obtain the η -nucleus optical potential at finite nuclear density as,

$$V_\eta(\omega, \rho(r)) = \frac{g_\eta^2}{2\mu\omega + m_N^*(\rho) - m_{N^*}^*(\rho) + i\Gamma_{N^*}(\omega, \rho)/2}, \quad (3)$$

in the local density approximation and the heavy baryon limit [32]. Here μ is the η -nucleus reduced mass and $\rho(r)$ is the density distribution of the nucleus. The ηNN^* coupling is assumed to be S -wave:

$$\mathcal{L}_{\eta NN^*}(x) = g_\eta \bar{N}(x)\eta(x)N^*(x) + \text{H.c.}, \quad (4)$$

and the coupling constant g_η is determined to be $g_\eta \simeq 2.0$ in order to reproduce the partial width $\Gamma_{N^* \rightarrow \eta N} \simeq 75\text{MeV}$ at tree level. The S -wave nature of the ηNN^* vertex simplifies the particle-hole loop integral in Eq. (3). m_N^* and m_{N^*} are the effective masses of N and N^* in the nuclear medium, respectively. Considering that the N^* mass in free space lies only 50 MeV above the threshold and that the mass difference of N and N^* might change in the medium, the η -nucleus optical potential is expected to be extremely sensitive to the in-medium properties of N and N^* . For instance, if the mass difference reduces in the nuclear medium as $m_\eta + m_N^* - m_{N^*} > 0$, then the optical potential turns to be repulsive [6].

Using the free space values of the N and N^* masses in Eq. (3), we find that the optical potential gives an attractive ηN scattering length, $a_\eta = 0.24 + i0.38$ fm, which is comparable to $a_\eta = 0.20 + i0.26$ fm and $a_\eta = 0.26 + i0.25$ fm as reported in Ref. [39, 40], respectively. On the other hand, the value of the ηN scattering length a_η of our model is smaller than the recent analyses, in which larger values are reported such as $a_\eta \sim 0.9 + i0.3$ fm [41, 42]. In the present study, however, our main purpose is to study the effects of the partial restoration of chiral symmetry in medium. As we shall see below, in the chiral doublet scenario of N and N^* , the repulsive η -nucleus interaction can be realized in the nuclear medium due to the symmetry restoration. This exotic behavior of the η -nucleus interaction is independent of the absolute value of a_η in our model. Thus, we start with the optical potential (3) and take into account the effects of the chiral symmetry restoration properly to N^* and the η -mesic nuclei.

The chiral doublet model is used for the calculation of the in-medium masses of N and N^* and the in-medium N^* width in Eq. (3). The Lagrangian of the chiral doublet model (the mirror model) is given as [36, 37],

$$\begin{aligned} \mathcal{L} = & \sum_{i=1,2} \left[\bar{N}_i i \not{\partial} N_i - g_i \bar{N}_i (\sigma + (-)^{i-1} i \gamma_5 \vec{\tau} \cdot \vec{\pi}) N_i \right] \\ & - m_0 (\bar{N}_1 \gamma_5 N_2 - \bar{N}_2 \gamma_5 N_1) + \mathcal{L}_{\text{meson}} \end{aligned} \quad (5)$$

where the nucleon fields N_1 and N_2 have positive and negative parities, respectively, and the physical nucleons N and N^* are expressed as a linear combination of N_1 and N_2 . The parameters are determined so that the model reproduces the free space values of the N and N^* masses and the partial decay width of N^* to πN as $\Gamma_{N^* \rightarrow \pi N} = 75$ MeV with $\langle \sigma \rangle_0 = 93$ MeV [37].

In the chiral doublet model together with the assumption of partial restoration of chiral symmetry, a reduction of the mass difference of N and N^* in the medium is found to be in the mean field approximation as [36, 37, 43, 44],

$$m_N^*(\rho) - m_{N^*}^*(\rho) = \Phi(\rho)(m_N - m_{N^*}), \quad (6)$$

where m_N and m_{N^*} are the N and N^* masses in free space, respectively, and

$$\Phi(\rho) = 1 - C \frac{\rho}{\rho_0}. \quad (7)$$

Here we take the linear density approximation of the in-medium modification of the chiral condensate, and the parameter C represents the strength of the chiral restoration at the nuclear saturation density ρ_0 . The empirical value of C lies from 0.1 to 0.3 [27]. Here we perform our calculations with $C = 0.0$ and 0.2 in order to investigate the effect of the partial restoration of chiral symmetry. A self-consistent calculation within the chiral doublet model gives moderately linear dependence of the chiral condensate to the density with $C = 0.22$ in Ref. [44], in which the relativistic Hartree approximation is used to calculate the chiral condensate in nuclear matter.

In Fig. 1, we show the η -nucleus optical potentials obtained by the chiral doublet model with $C = 0.0$ and $C = 0.2$ in the case of the η - ^{11}B system assuming the local density approximation and the Woods-Saxon nuclear distribution defined in Eq. (2). The potential with $C = 0.0$ corresponds to the so-called $t\rho$ approximation because there are no medium modifications for N and N^* . As shown in the figure, the potential with $C = 0.2$ has quite different shape from the case with $C = 0.0$. The η -nucleus optical potential with $C = 0.2$ turns to be repulsive above a critical density ρ_c at which the sign of $\omega + m_N^* - m_{N^*}^*$ becomes positive. Consequently, the η -nucleus optical potential has a curious shape of a repulsive core inside nucleus and an attractive pocket in nuclear surface as indicated in Fig.1. The

qualitative feature of the optical potential discussed here, such as the appearance of the repulsive core in the case of $C = 0.2$, is independent of type of nuclei due to saturation of nuclear density. It is extremely interesting to confirm the existence (or non-existence) of this curious shaped potential experimentally.

We should mention here that there are two types of the chiral doublet model, namely, the mirror assignment and the naive assignment, due to two possible type of assignment for the axial charge to the N and N^* [36,37]. The potential in Fig. 1 is obtained by the mirror assignment case. In the mirror assignment, N^* is regarded as the chiral partner of N and forms a chiral multiplet together with N . While in the naive assignment, N and N^* are treated as independent baryons in the sense of the chiral group. We calculate the reaction spectra using both assignments, and show the results in next section. In both cases, the mass difference of N and N^* is given in the same form as shown in Eq. (6). Hence, the energy and the density dependence of the potential of the naive assignment resemble those of the mirror assignment. The detail discussions are given in Ref. [7].

Let us move on the second approach of the chiral unitary model [15, 39]. In this approach, the N^* resonance is expressed as a dynamically generated object in the meson baryon scattering, and one solves a coupled channel Bethe-Salpeter equation to obtain the η -nucleon scattering amplitude. The optical potential in medium is obtained by closing the nucleon external lines in the ηN scattering amplitude and considering the in-medium effect on the scattering amplitude, such as Pauli blocking. Since the N^* in the chiral unitary approach is found to have a large component of $K\Sigma$ and the Σ hyperon is free from the Pauli blocking in nuclear medium, very little mass shift of N^* is expected in the medium [45], while the chiral doublet model predicts the significant mass reduction as discussed above. The optical potential obtained by the chiral unitary approach in Ref. [15] is also shown in Fig. 1, and the potential resembles that of the chiral doublet model with $C = 0.0$ due to the small medium effect.

In Ref. [6], in order to obtain the eigenenergies, we have solved the Klein-Gordon equation Eq. (1) numerically with the η -nucleus optical potential given in Eq. (3) for the mirror assignment. We show in Table 1 the calculated binding energies and level widths for $0s$ and $0p$ states in the ^{11}B and ^{39}K cases. We also show in Table 1 the binding energies and widths by the chiral unitary approach reported

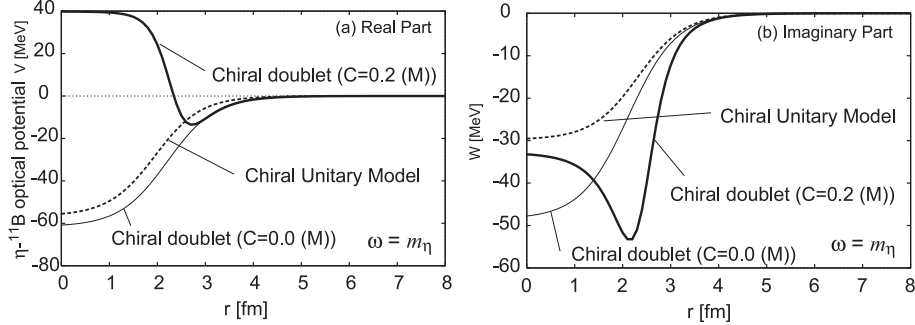


Figure 1: The η -nucleus optical potential for the η - ^{11}B system as functions of the radius coordinate r reported in Ref. [7]. The left and right figures show the real part and the imaginary part of the η -nucleus optical potential, respectively. In both figures, the solid lines show the potentials of the chiral doublet model with $C = 0.2$ (thick line) and $C = 0.0$ (thin line), and dashed lines show that of the chiral unitary model, which is picked from the results shown in Ref. [15]

in Ref. [15] for comparison. The level structure of the bound states is qualitatively very similar with that of the chiral doublet model with $C = 0.0$ as we can expect from the potential shape. For the $C = 0.2$ case in the chiral doublet model, we can not find any bound states because of the repulsive nature of the optical potential.

2.2 ω -nucleus optical potential

Let us move to discussion on the optical potential of in-medium ω meson. In our study of the ω mesic nuclei, we use a simple model for the optical potential, which was used in the previous study [9] on the ω -mesic nuclei formation using the $(d, ^3\text{He})$ reaction. An empirical potential is given in an energy-independent $T\rho$ approximation as

$$V_{\omega}^{(a)}(r) = -(100 + 70i) \frac{\rho(r)}{\rho_0}. \quad (8)$$

The real and imaginary parts of the optical potential were estimated based on 15 % mass reduction of the ω mass at the normal density and the ω life time ($\tau = 1.5 \text{ fm}/c$) of nuclear absorption in the nuclear medium, respectively, as reported in Ref. [16].

Chiral doublet model with C=0.0 [MeV]		Chiral doublet model with C=0.2	
^{11}B	^{39}K	^{11}B	^{39}K
0s	(13.7, 41.5)	(30.3, 42.5)	<i>no bound state</i>
0p	-	(14.6, 50.7)	

Chiral unitary approach [15] [MeV]	
^{12}C	^{40}Ca
0s	(9.71, 35.0)
0p	(7.0, 38.6)

Table 1: Binding energies and widths calculated by the Chiral Doublet model (C=0.0 and C=0.2) with the mirror assignment [6] and by the chiral unitary approach reported in Ref. [15].

ω - ^{11}B bound states	$V_{\omega}^{(a)}$	$V_{\omega}^{(b)}$
0s	(49.0, 116)	(103, 54.4)
1s	-	(18.8, 27.6)
0p	(14.3, 86.5)	(58.1, 42.7)
0d	-	(17.0, 30.5)

Table 2: Binding energies and widths of the ω bound states in ^{11}B with the optical potentials (8) and (9) in unit of MeV.

The binding energies and widths of the omega meson in ^{11}B are calculated by solving the Klein-Gordon equation (1) with the above potential. In this potential, we find two bound states in the ^{11}B nucleus. The obtained binding energies and widths are shown in Table 2. Since the width of these states are larger than the level spacing, it would be difficult to observe distinct peak structure in inclusive spectra. In next section, we will show the calculated (γ, p) spectra for several incident energies.

We also consider two more optical potentials in order to investigate the sensitivity of the depth and the absorption of the potential to the (γ, p) spectra. The potentials considered here are

$$V_{\omega}^{(b)}(r) = -(156 + 29i) \frac{\rho(r)}{\rho_0}, \quad (9)$$

$$V_{\omega}^{(c)}(r) = -(-42.8 + 19.5i) \frac{\rho(r)}{\rho_0} \quad (10)$$

which are obtained by the linear density approximation with the scattering lengths $a = 1.6 + 0.3i$ fm [17] and $a = -0.44 + 0.2i$ fm [25], respectively. The former scattering length is obtained by the ωN scattering amplitude calculated at one loop approximation with an effective Lagrangian based on the SU(3) chiral symmetry incorporating vector mesons. On the other hand, the later is obtained in a relativistic and unitary approach for meson-baryon amplitudes. In this case the scattering length is to be repulsive due to a subthreshold effect of the $\omega N(1520)$.

The energies and widths of the bound states calculated with the potential $V_{\omega}^{(b)}$ are also shown in Table 2. In this case, more bound states are found with relatively narrower widths than the case of the previous potential $V_{\omega}^{(a)}$ since the optical potential $V_{\omega}^{(b)}$ has deeper real potential and less nuclear absorption. The magnitudes of the level widths are comparable to those of level spacing and, hence, we expect to observe peak structure in reaction spectra. Later we shall compare the (γ, p) spectra calculated with these potentials at the incident energy $E_{\gamma} = 2.7$ GeV where the recoilless condition is satisfied.

2.3 σ -nucleus optical potential

Finally, we consider the σ meson-nucleus systems. In this paper we take a particle picture of the sigma meson, in which the sigma meson is described as a particle with a huge decay width to two pions. The calculation of the self-energy of the sigma meson is performed based on the SU(2) linear sigma model [27], and the partial restoration of chiral symmetry in nuclear medium is parameterized as the sigma condensation in the medium within the model.

The optical potential for the σ -nucleus is defined as the density-dependent part of the in-medium σ self-energy divided by two times the bare sigma mass m_{σ} as;

$$\text{Re}V_{\sigma}(\omega, \rho) = -\frac{1}{2m_{\sigma}} \lambda \sigma_0^2 (1 - \Phi(\rho)). \quad (11)$$

Here we use the σ self-energy evaluated in Ref. [27] based on the SU(2) linear sigma model at the one-loop level, which corresponds to the mean field approximation. The density dependent function $\Phi(\rho)$

is defined to express the chiral condensate in nuclear matter $\langle\sigma\rangle_\rho$ as $\langle\sigma\rangle_\rho = \sigma_0\Phi(\rho)$. The function $\Phi(\rho)$ is given in Eq.(7) with the C parameter, which represents the strength of the partial restoration of the chiral symmetry in the nuclear medium. It is worth noting that at the one-loop approximation the imaginary part of the self-energy is independent of the density, so that the nuclear absorption of the sigma meson appears from the next order, such that multi- ph excitations and pion - ph excitations.

The density-independent part of the self-energy Σ_σ is given in the one-loop calculation in the linear sigma model as

$$\begin{aligned} \text{Re}\Sigma_\sigma(\omega) = & - \frac{\lambda}{32\pi^2} \left[m_\pi^2 \left(1 - \ln \frac{m_\pi^2}{\kappa^2}\right) + m_\sigma^2 \left(1 - \ln \frac{m_\sigma^2}{\kappa^2}\right) \right. \\ & + \frac{1}{3} \lambda \sigma_0^2 \left(Q_\pi + 2 - \ln \frac{m_\pi^2}{\kappa^2} \right) \\ & \left. + \lambda \sigma_0^2 \left(Q_\sigma + 2 - \ln \frac{m_\sigma^2}{\kappa^2} \right) \right], \end{aligned} \quad (12)$$

$$\text{Im}\Sigma_\sigma(\omega) = - \frac{\lambda^2}{32\pi} \sigma_0^2 \left[\frac{1}{3} P_\pi \theta(\omega - 2m_\pi) + P_\sigma \theta(\omega - 2m_\sigma) \right], \quad (13)$$

where the function Q_φ is given as

$$Q_\varphi = \begin{cases} P_\varphi \ln \frac{1 - P_\varphi}{1 + P_\varphi} & (\text{for } 2m_\varphi \leq \omega) \\ -2P_\varphi \arctan \frac{1}{P_\varphi} & (\text{for } \omega \leq 2m_\varphi) \end{cases}, \quad (14)$$

with $P_\varphi = \left|1 - 4m_\varphi^2/\omega^2\right|^{1/2}$. Here, φ denotes either π or σ , κ is a renormalization point in the minimal subtraction scheme and λ is the coupling constant of the four-point meson vertex in the linear sigma model. The reduced mass μ shown in the Klein-Gordon equation (1) is corresponding to $\mu^2 = m_\sigma^2 + \text{Re}\Sigma_\sigma$ in heavy nucleus limit for the sigma meson case. The bare sigma mass m_σ is fitted as 469 MeV so that the sigma meson mass in free space $m_\sigma^{(\text{free})}$ is reproduced as 550 MeV after the one-loop calculation. All parameters appeared in Eqs. (12)-(14) are obtained in the first reference of Ref. [26] and listed in Table.1 of Ref. [18].

The self-energy of the sigma meson obtained in the mean field provides a strong attractive potential for the sigma meson in medium. We

show in Fig. 2 the attractive potential $\text{Re}V_\sigma(r)$, given in Eq.(11), for $C = 0.2, 0.3$ and 0.4 in ^{208}Pb . We assume that the density distribution is of the Woods-Saxon type as defined in Eq. (2) with $R = 6.5$ fm and $a = 0.5$ fm. It is seen that the depth of the attractive potential is strongly depend on the C parameter. The strong attraction of the optical potential in the center of nucleus appears also in lighter nuclei.

As a result of the attraction, we expect that a strong reduction of the σ mass approaching down to the two pion threshold especially for heavy nuclei. Consequently there is a chance to form sigma bound states with narrower widths. The reduction of the sigma mass in nuclear medium is expected also in the $\pi\pi$ resonance picture of the sigma meson with the non-linear realization of chiral symmetry, if one takes account of appropriate medium effects through the pion wave function renormalization [28].

The energies and widths of the sigma bound states are calculated by solving the Klein-Gordon equation for the σ meson with the optical potential V_σ and the self-energy Σ_σ with the one-loop correction. In Fig. 3, we show the bound state spectra of the σ meson in ^{208}Pb with $C = 0.2, 0.3$ and 0.4 cases, together with widths of low lying states [18]. It is found that, if the partial restoration of chiral symmetry in nuclear medium occurs with sufficient strength, deeply bound σ states in heavy nuclei formed with significantly smaller decay widths than that in vacuum. This is responsible for suppression of the available $\pi\pi$ phase space associated with the reductions of the real energies of the bound states. Furthermore, for $C = 0.3$ and 0.4 cases, there are several bound states with no decay widths below the 2π threshold since the $\sigma \rightarrow \pi\pi$ decay channel, which is the only possible decay mode at low energies in the present model, is kinematically forbidden.

In order to see a global structure of the σ bound states in the nucleus and the impact of the narrow bound states on the production reaction, we show the spectral functions of the bound states, which are used to calculate the σ production spectra in the (γ, p) reaction later. The spectral function of the (n, ℓ) bound state is given by

$$\rho_{n\ell}(\omega) = -\frac{1}{\pi} \frac{\text{Im}\Sigma_\sigma(\omega)}{(\omega^2 - \omega_{n\ell}^2)^2 + (\text{Im}\Sigma_\sigma(\omega))^2}, \quad (15)$$

where $\omega_{n\ell}$ denotes the eigenenergy of the σ bound state in the nucleus. The spectral functions Eq. (15) encounter a divergence at $\omega = \omega_{n\ell}$ for eigenstates in case of $\text{Im}\Sigma_\sigma = 0$. This is not the case if we take

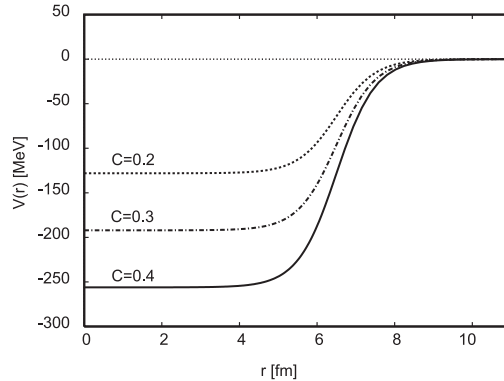


Figure 2: Real potential for the σ meson inside the ^{208}Pb nucleus as a function of the radial coordinate r obtained in Ref. [18]. The density is assumed to be the Woods-Saxon form with $R = 6.5$ fm and $a = 0.5$ fm in Eq. (2). Each line indicates $C = 0.2$ (dotted line), 0.3 (dot-dashed line) and 0.4 (solid line) case, respectively.

into account nuclear absorptions of the sigma meson which we do not consider here. In order to regularize the divergence, we add an extra 5 MeV width to the $\text{Im}\Sigma_\sigma$ in all the bound states in the following calculations.

Figure 4 shows a series of ρ_{nl} for the $\ell = 0$ bound states in ^{208}Pb for the $C = 0.3$ case [18]. As seen in the figure, the spectral functions for the deeply bound states have a prominent peak around $\omega \sim 2m_\pi$. This is a direct consequence that the deep bound states are formed as a result of the strong attractive potential. The detail discussions are given in Ref. [18]. The appearance of the narrow states at the low energies gives also strong enhancement of the sigma production rate in nucleus around the two pion threshold, which is expected to be seen in the (γ, p) reaction. This point is discussed in the following section.

It is also possible to form the deeply bound states with the narrow width in lighter nuclei than Pb, since the potential depth is nearly independent of the mass number of nucleus for a certain value of the C parameter. The spatial range of the potential, however, depends on nuclear size. Therefore, the zero width bound states are expected to be formed in nuclei which are larger than a certain spatial dimension.

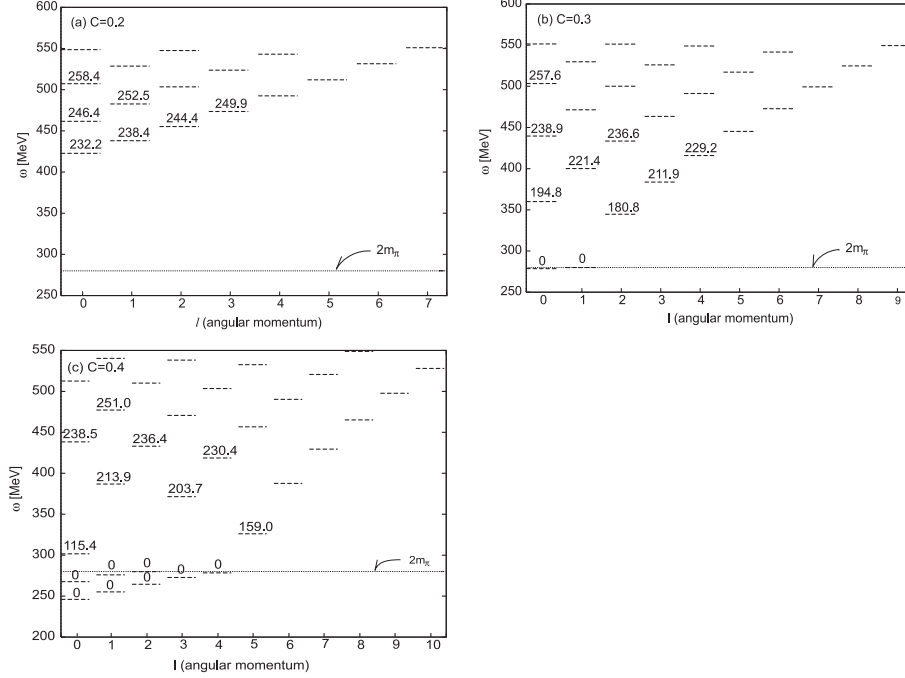


Figure 3: Calculated eigenenergies of the bound σ in ^{208}Pb [18] with (a) $C = 0.2$, (b) $C = 0.3$ and (c) $C = 0.4$. The ℓ is the orbital angular momentum of the σ states. Widths are shown by numbers for low lying states in unit of MeV. The $2m_\pi$ threshold is shown by the dotted line. The states below the threshold do not have widths due to the $\pi\pi$ decay in the present calculation.

3 Formation of meson-nucleus system in (γ, p) reaction

In this section we explain the advantages of the (γ, p) reaction for investigation of the meson-nucleus system and briefly review the formulation to obtain the formation rate of the mesons inside nucleus.

3.1 (γ, p) reaction

In the (γ, p) reaction, the incident photon reacts with a proton inside the target nucleus, producing a meson there most likely at rest with recoilless condition. The meson may be trapped into a certain bound

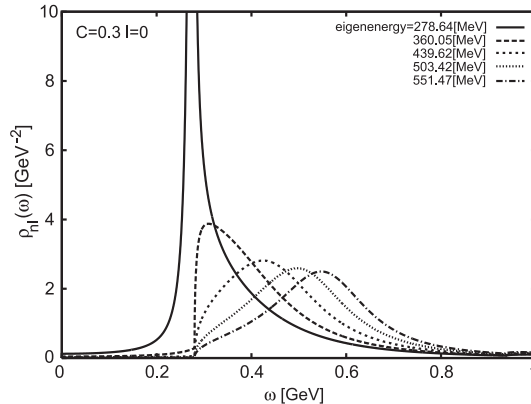


Figure 4: Spectral functions $\rho_{n\ell}(\omega)$ of the σ bound states with $\ell = 0$ and $n = 1, 2, \dots, 5$ for $C = 0.3$ case obtained in Ref. [18]. An extra 5 MeV width is added to the imaginary part of the self-energy.

state in the nucleus, if there exist bound states. The proton is ejected from the nucleus and is to be observed at a forward angle. In the (γ, p) reaction spectroscopies, one observes only the emitted proton in the final state for simplicity of the experiment and obtains the double differential cross section $d\sigma/d\Omega/dE$ as a function of the emitted proton energy. Investigating the differential cross section, we extract the properties of the interaction between each meson and the nucleus. Observing the more particles in the final state, we will obtain the more information of the meson-nucleus interactions.

The incident energy for each meson production is tuned so as to satisfy the recoilless condition achieved by the zero momentum transfer, in which the meson may be produced in the nucleus at rest. In the recoilless condition, due to the matching condition between momentum- and angular momentum-transfer, we have a selection rule for the total angular momentum of the meson and the proton hole states. Namely the contributions of the different angular momenta are strongly suppressed.

In Fig. 5, we show the momentum transfers as functions of the incident particle energies for the $(d, {}^3\text{He})$ and (γ, p) reactions. In the plots we use the meson masses in free space. In the following discussion for the (γ, p) reaction we choose the incident energy $E_\gamma = 950$ MeV for the eta meson production and $E_\gamma = 2.75$ GeV for the omega meson

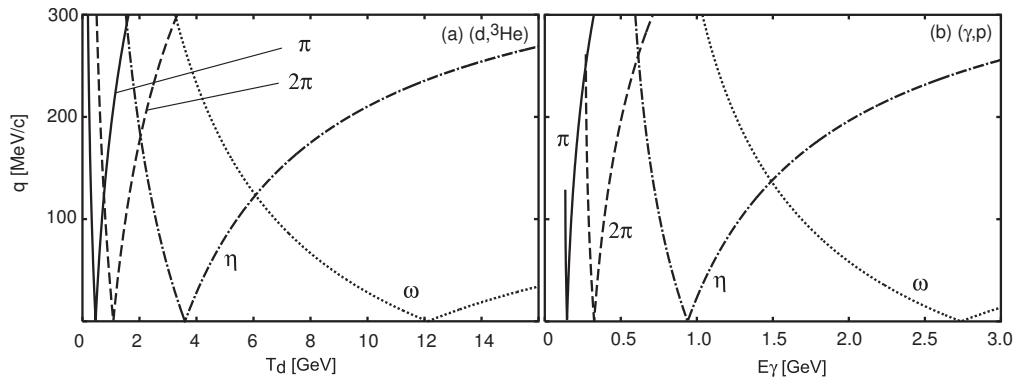


Figure 5: Momentum transfer q is shown as a function of (a) the incident deuteron kinetic energy T_d in the $(d, {}^3\text{He})$ reaction, and (b) the incident γ energy E_γ in the (γ, p) reaction. The solid line shows the momentum transfer of the pion production case, and other lines show those of two pions, the η meson and the ω meson production cases as indicated in the figure.

production to satisfy the recoilless condition for the corresponding meson-nucleus systems. For the sigma meson case, the incident energy is chosen to be $E_\gamma = 400$ MeV, which is a recoilless condition for the two pion production in the nucleus, since we focus our interest on the spectral function enhancement near the two pion threshold in the sigma channel associated with the partial restoration of chiral symmetry in nuclear medium.

The major advantage of use of the (γ, p) reaction for the mesic nucleus formation is the smaller distortion effect on the incident photon than hadronic beams. The distortion effects of the projectile and ejectile are known to reduce significantly the reaction rate inside the nucleus. As we shall discuss later in Fig.6, half of the flux of the (γ, p) reaction reaches the center of the target nucleus, while most of the flux in the $(d, {}^3\text{He})$ reaction is restricted on the surface of the nucleus. Therefore, due to the transparency of photon, we can probe the meson wavefunction in the center of the nucleus with the (γ, p) reaction. This characteristic feature is desirable especially to the study of the eta-nucleus system, in which we have the discrepancy in the model calculations of the η optical potential at the center of the nucleus depending on the physical picture of N^* , as discussed in Sec.2.1

The other advantage of the (γ, p) reaction is that, due to the trans-

parency of photon, we expect more production rate of the low lying states of the mesic nucleus. This is favorable to the sigma-nucleus system, since we expect the deeply bound states of the sigma meson with a significantly narrow width as a result of strong reduction of the chiral condensate in the nucleus. In the case of mesic nuclei formation, the meson wave function in nucleus resembles the proton hole wave function in the sense of function orthogonality, because both of the wave functions are, roughly to say, solutions of the Schrödinger equations with the same square-well type potentials. (Recall that the potentials for the mesons is obtained as the Woods-Saxon type shape under the local density assumption with the nuclear density distribution (2) except the case of the eta meson with the chiral doublet model $C = 0.2$.) Due to the orthogonality of the wave functions, we have the selection rule that the combinations of the different principle quantum numbers of the meson and proton hole wave functions are strongly suppressed in the recoilless condition [9, 18]. This is reminiscent of the recoilless formation of substitutional states in hypernuclear reactions. Therefore, in order to produce the ground state of the mesic nucleus, in which the meson sits on the s state, we need to pick up the deepest bound proton from the target nuclei using a better transparent incident beam. In contrast, in the case of the atomic state formation, the orthogonal condition of the radial wave functions of the meson and nucleon is not satisfied any more, since the meson is trapped in a Coulomb potential and the meson distribution is roughly expressed by the Coulomb wave function. Then the recoilless condition enhances the population of any states which have the total angular momentum $J \sim 0$, for example, in the formation of the deeply bound pionic atoms in Sn isotopes [5, 46], the contribution of $(3s)_n^{-1} \otimes 1s_\pi$ combination can be largely populated in the $(d, {}^3\text{He})$ reaction.

Let us evaluate the distortion effects of the $(d, {}^3\text{He})$ and (γ, p) reactions to compare the 'transparency' of both reactions. We describe the distorted waves of the incoming projectile and of the outgoing ejectile as χ_i and χ_f , respectively. Using the Eikonal approximation, we write

$$\chi_f^*(\mathbf{r})\chi_i(\mathbf{r}) = \exp(i\mathbf{q} \cdot \mathbf{r})F(\mathbf{r}), \quad (16)$$

with the momentum transfer \mathbf{q} . We choose the beam direction as to be z -axis. The momentum transfer \mathbf{q} is along z -axis in the forward reactions which we consider here. The distortion factor $F(\mathbf{r})$ is defined

as,

$$F(\mathbf{r}) = \exp \left[-\frac{1}{2}\sigma_{iN} \int_{-\infty}^z dz' \rho_A(z', b) - \frac{1}{2}\sigma_{fN} \int_z^{\infty} dz' \rho_{A-1}(z', b) \right]. \quad (17)$$

where σ_{iN} (σ_{fN}) is the total cross section of the nucleon and incident (emitted) particle and $\rho_A(z, b)$ is the density distribution function for the nucleus with the mass number A in the coordinates of $z = r \cos \theta$ and $b = r \sin \theta$. The distortion factor, which will be used in the calculation of the (γ, p) reaction cross section later, gives an estimation of the reduction of the beam flux caused by the nuclear absorption effects. In order to take a view of the distortion effect, we calculate an averaged distortion factor, which is defined as

$$\bar{F}(b) = \exp \left[-\frac{1}{2}\bar{\sigma} \int_{-\infty}^{\infty} \bar{\rho}(z', b) dz' \right], \quad (18)$$

where $\bar{\sigma}$ is an average distortion cross section of the initial and final channels, and $\bar{\rho}(z, b)$ denotes an average nuclear density of the target and daughter nuclei at an impact parameter b and a beam direction coordinate z .

In Fig. 6, we show the averaged distortion factors $\bar{F}(b)$ in the (γ, p) reaction and the $(d, {}^3\text{He})$ reaction of the ${}^{12}\text{C}$ target case for η production, which will be discussed in Sec. 4.1. Here we have used $\bar{\sigma} = 104$ mb for the $(d, {}^3\text{He})$ reaction and $\bar{\sigma} = 16$ mb for the (γ, p) reaction. These cross sections are evaluated from experimental nucleon-nucleon scattering data at appropriate energies [47]. The figure shows that $\bar{F}(b)$ in the (γ, p) reaction has a finite value (≥ 0.5) even in the nuclear center. This means that the amplitude of the meson production at center of nucleus is suppressed only by half due to the nuclear absorption. On the other hand, the averaged distortion factor of the $(d, {}^3\text{He})$ reaction is almost zero inside the nucleus. Therefore the photon can reach the center of the nucleus and create the meson there, while the deuteron mostly creates meson only on the surface of the nucleus. Thus, as we expected, the (γ, p) spectra are shown to be more sensitive to the optical potential of the meson at the interior of the nucleus.

3.2 Formulation

We use the Green function method [21] to calculate the formation cross sections of the η -nucleus and the ω -nucleus systems in the (γ, p)

reaction. The details of the application of the Green function method for the (d,³He) reaction are found in Refs. [6, 9, 17].

The present method starts with a separation of the reaction cross section into the nuclear response function $S(E)$ and the elementary cross section of the $p(\gamma,p)\eta$ or ω with the impulse approximation:

$$\left(\frac{d^2\sigma}{d\Omega dE}\right)_{A(\gamma,p)(A-1)\otimes\varphi} = \left(\frac{d\sigma}{d\Omega}\right)_{p(\gamma,p)\varphi}^{\text{lab}} \times S(E), \quad (19)$$

where φ denotes the η or ω meson. The calculation of the nuclear response function with the complex potential is formulated by Morimatsu and Yazaki [21] in a generic form as

$$S(E) = -\frac{1}{\pi} \text{Im} \sum_f \mathcal{T}_f^\dagger G(E) \mathcal{T}_f \quad (20)$$

where the summation is taken over all possible final states. The amplitude \mathcal{T}_f denotes the transition of the incident particle to the proton hole and the outgoing ejectile, involving the proton hole wavefunction ψ_{j_p} and the distorted waves, χ_i and χ_j , of the projectile and ejectile, taking the appropriate spin sum:

$$\mathcal{T}_f(\mathbf{r}) = \chi_f^*(\mathbf{r}) \xi_{1/2, m_s}^* \left[Y_{l_\varphi}^*(\hat{r}) \otimes \psi_{j_p}(\mathbf{r}) \right]_{JM} \chi_i(\mathbf{r}) \quad (21)$$

with the meson angular wavefunction $Y_{l_\varphi}(\hat{r})$ and the spin wavefunction $\xi_{1/2, m_s}$ of the ejectile. The distorted waves are written with the distortion factor as Eq.(16) in the Eikonal approximation. The Green function $G(E)$ contains the meson-nucleus optical potential in the Hamiltonian as

$$G(E; \mathbf{r}, \mathbf{r}') = \langle p^{-1} | \phi_\varphi(\mathbf{r}) \frac{1}{E - H_\varphi + i\epsilon} \phi_\varphi^\dagger(\mathbf{r}') | p^{-1} \rangle \quad (22)$$

where ϕ_φ^\dagger is the meson creation operator and $|p^{-1}\rangle$ is the proton hole state. Obtaining the Green function with the optical potential is essentially same as solving the associated Klein-Gordon equation. We can calculate the nuclear response function $S(E)$ from $\mathcal{T}_f^\dagger(\mathbf{r}) G(E; \mathbf{r}, \mathbf{r}') \mathcal{T}_f(\mathbf{r}')$ by performing appropriate numerical integrations for variables \mathbf{r} and \mathbf{r}' .

For the σ -nucleus systems, we do not use the Green function method to evaluate the formation rate, because (a) we do not know

the elementary cross section of the $\gamma + p \rightarrow \sigma + p$ reaction yet and (b) the sigma optical potential has a large imaginary part even outside of the nucleus due to the large decay width, of which boundary condition the Green function does not work in the present formalism. Alternatively we evaluate the spectral function of the σ bound states defined as

$$\rho_\sigma(E) = \sum_{n,\ell} (2\ell + 1) \rho_{n\ell}(E) , \quad (23)$$

where $\rho_{n\ell}(E)$ denotes the contribution from each bound state in the nucleus with the (n, ℓ) quantum number as given in Eq. (15). In order to take the reaction mechanism into consideration, we introduce an effective number N_{eff} , which represents relative production weight of each bound state [2, 18]. Finally we obtained the total spectral function as

$$\rho_{\text{tot}}(\omega) = \sum_{n\ell} N_{\text{eff}} \rho_{n\ell}(\omega). \quad (24)$$

with the effective number N_{eff} given by

$$N_{\text{eff}} = \sum_{JMm_s} \left| \int d^3r \chi_f^*(\mathbf{r}) \xi_{1/2, m_s}^* [\phi_{\ell\sigma}^*(\mathbf{r}) \otimes \psi_{j_n}(\mathbf{r})]_{JM} \chi_i(\mathbf{r}) \right|^2 \quad (25)$$

where ψ_{j_p} denotes the wave function of the picked-up proton and, $\phi_{\ell\sigma}$ and $\xi_{1/2, m_s}$ are the σ wave function and the spin wave function of the ejectile, respectively. The σ wave function is obtained by solving the Klein-Gordon equation with the optical potential and the self-energy shown in Eqs. (11), (12) and (13).

This effective number approach is known to be a good approximation of the Green function method to calculate the reaction cross section in Eq.(19), if the bound states lie well-separately with narrow widths [21], and applied to evaluate the formation cross sections of deeply bound pionic atoms [2]. In the present case of the sigma meson in nucleus, we expect the narrow bound states around the two-pion threshold for the $C = 0.3$ and $C = 0.4$ cases, and focus our interest on seeing the impact of the narrow bound states on the (γ, p) reaction. Therefore the approach with the spectral function is expected to be reasonable for our purpose.

4 Result

In this section, we evaluate the formation rates of the mesic nuclei by the (γ, p) reactions and show the spectra calculated with the optical potentials discussed in Section 2 for the η -, ω -, and σ -nucleus systems.

4.1 η -nucleus system

We discuss in this section the formation rate of the η -mesic nucleus in the (γ, p) reaction. The initial photon energy is chosen as the recoilless condition energy $E_\gamma = 950$ MeV as shown in Fig. 5(b). The emitted proton spectra around the η production energies are evaluated in the Green function method (19) with the η Green function (22) calculated with the optical potential (3). We estimate the elementary cross section $d\sigma/d\Omega$ of the $\gamma + p \rightarrow p + \eta$ reaction at this energy in the laboratory frame as to be $3.4\mu\text{b/sr}$ using the experimental data by the tagged photon beam at University of Tokyo [48].

The obtained spectra are shown as functions of the excitation energy E_{ex} measured from the eta meson production threshold energy E_0 . The excitation energy corresponds to the missing energy in the inclusive reaction $\gamma + A \rightarrow p + X$. In the plot of the separated contributions of the η -hole configurations, it should be taken into account the appropriate hole energy depending on the orbit j_p in the daughter nucleus. The hole energy $S_p(j_p) - S_p(\text{ground})$ is measured from the ground state of the daughter nucleus, which are listed in Table 3. The binding energy B_η of the η meson is deduced from the excitation energy and the hole energy as

$$E_{\text{ex}} = m_\eta - B_\eta + [S_p(j_p) - S_p(\text{ground})]. \quad (26)$$

We evaluate the differential cross section of the (γ, p) reaction on the ^{12}C target. The η meson is created in the ^{11}B nucleus because the proton is knocked out in the reaction. In Fig. 7, we show the results calculated by the chiral doublet model with both mirror and naive assignments together with those of the $(d, ^3\text{He})$ reaction reported in [6, 7] for $C = 0.2$ case in Eq.(7).

First of all we would like to mention that the peak structure seen in the spectra has nothing to do with the existence of the η bound states. (Actually in the case of $C = 0.2$ there are no bound states.) These

^{12}C	j_p	$S_p(j_p) - S_p(1p_{3/2})$	Γ_{j_p}
	$1p_{3/2}$	0	-
	$1s_{1/2}$	18	-
^{40}Ca	j_p	$S_p(j_p) - S_p(1d_{3/2})$	Γ_{j_p}
	$1d_{3/2}$	0	0
	$2s_{1/2}$	3.2	7.7
	$1d_{5/2}$	8.0	3.7
	$1p_{1/2}, 3/2$	24.9	21.6
	$1s_{1/2}$	48.0	30.6

Table 3: Proton separation energies of the single particle orbits measured from the ground state of the daughter nucleus are shown in unit of MeV. Data taken from Ref. [49] for ^{12}C and Ref. [50] for ^{40}Ca . Widths of the proton hole states deduced from the data are also shown for ^{40}Ca .

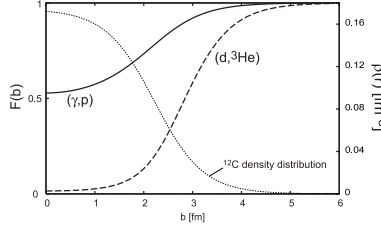


Figure 6: Distortion factor $\bar{F}(b)$ for the η meson production reactions in ^{12}C target as a function of the impact parameter b . The solid line indicates the $\bar{F}(b)$ for the (γ, p) reaction and the dashed line for the $(d, ^3\text{He})$ reaction. The density profile of ^{12}C is also shown.

peaks are just signals of opening the phase space of the η creation in the nucleus [7].

Secondly we see in the figure that each spectrum is dominated by two contributions, $(0s_{1/2})_p^{-1} \otimes s_\eta$ and $(0p_{3/2})_p^{-1} \otimes p_\eta$. This is a consequence of the matching condition in the recoilless kinematics that final states with total spin $J \neq 0$ are largely suppressed. The η production threshold for the $(0p_{3/2})_p^{-1}$ proton-hole state is indicated as vertical thin line at $E_{\text{ex}} - E_0 = 0$. The threshold for the $(0s_{1/2})_p^{-1}$ hole state, which is the excited state of the daughter nucleus, is at $E_{\text{ex}} - E_0 = 18$ MeV because of the different $S_p(j_p)$ in Eq. (26).

As we can see in the figure, the difference between the naive and

mirror assignments is enhanced in the (γ, p) reaction, as compared with the $(d, {}^3\text{He})$ case and, hence, the (γ, p) reaction is more sensitive to the details of the η -nucleus interaction as we expected. However, it might be difficult to distinguish these two cases by experimental data, since the difference is seen only in the magnitude of the spectra above the η production threshold. Hereafter, we show only the results with the mirror assignment.

In Fig. 8, we show again the ${}^{12}\text{C}$ target cases for the (γ, p) and $(d, {}^3\text{He})$ reactions of the η mesic nucleus, comparing the three different η -nucleus optical potentials. In Fig. 8(a), the spectra with the so-called $t\rho$ optical potential are shown, which are calculated by putting $C = 0.0$ in the chiral doublet model. We show also the spectra obtained by the chiral doublet model with $C = 0.2$ in Fig. 8(b). Comparing (a) and (b) in the left-side figure, we find that the repulsive nature of the potential in the chiral doublet model with $C = 0.2$ makes the bump structure of the $(d, {}^3\text{He})$ spectrum broaden out to the higher energy region, as discussed in Ref. [6]. On the right-hand side in Fig. 8, the same ‘broadening effect’ is seen also in the (γ, p) reaction. We would like to stress here that this tendency to widen the spectra is seen more clearly in the (γ, p) spectra as a result of the transparency of the incident photon. In Fig. 8(c), we show the spectra calculated by the chiral unitary approach. We can see that the spectra of the chiral unitary approach are shifted to the lower energy region like in Figs. 8(a) as a result of the attractive potential. It is very interesting to see which of spectra, (b) or (c), is realized in experiment. It is also interesting to compare the spectra of the (γ, p) and $(d, {}^3\text{He})$ reactions in experimental observation, since we can expect to obtain the detail information of the η -nucleus interaction by the comparison of the both data which have different sensitivities to the nuclear surface and center.

As for the contributions from the bound η states in the (γ, p) reaction, in Fig. 8(a) and (c), we find a certain enhancement in the $(0s_{1/2})_p^{-1} \otimes s_\eta$ configuration as a bump structure below the $0s$ state eta production threshold, which is $E_{\text{ex}} - E_0 = 18$ MeV. This is the indication of the η meson bound in the $0s$ state, which is listed in Table 1. Although the bound state is more clearly seen in the (γ, p) reaction, in which we expect more reaction rates to pick up a proton in deeper states in the target nucleus, as discussed before, it is still hard to distinguish the bound state as a peak structure even in the

(γ, p) reaction due to the large width of the bound state and the larger contribution of $(0p_{3/2})_p^{-1}$ state.

Next we consider the heavier target ^{40}Ca for the formation of the η mesic nucleus. In this case, we have larger possibilities to have bound states and to observe larger medium effects. In Fig. 9, we show the calculated spectra of $^{40}\text{Ca}(\gamma, p)^{39}\text{K} \otimes \eta$ reaction using the chiral doublet model with $C = 0.0$ and $C = 0.2$ together with those of the $(d, ^3\text{He})$ reaction for comparison. As in the case of the ^{12}C target, we find larger difference between the spectra with $C = 0.0$ and $C = 0.2$ in the (γ, p) reaction than those in the $(d, ^3\text{He})$ reaction. In the $(d, ^3\text{He})$ spectra, the total spectra are shifted around 5 MeV to higher excitation energy region with almost same shape by changing the C parameter value from $C = 0.0$ to $C = 0.2$. On the other hand, the (γ, p) spectra are largely shifted to higher energy region with significantly deformed shape. This is the good advantage of the (γ, p) reaction to deduce the information of the η optical potential. We can also see the contribution from the bound η states for the $C = 0.0$ case more clearly in the (γ, p) spectra. The bound states were obtained in the $C = 0.0$ case as energy 30.3 MeV with width 42.5 in s-wave and energy 14.6 with width 50.7 in p-wave [6]. However, as in the case of the $(d, ^3\text{He})$ reaction, it seems difficult to deduce the contribution from a certain subcomponent from the total spectra even in the (γ, p) reaction because of the large widths of the η states.

In short summary for the η mesic nucleus formation, we find that there exist certain discrepancies between the spectra obtained with the different chiral models and we also find that the (γ, p) spectra are more sensitive to these discrepancies than the $(d, ^3\text{He})$ spectra.

4.2 ω -nucleus system

In the ω production in the (γ, p) reactions, the recoilless condition is satisfied by the incident photon energy $E_\gamma = 2.75$ GeV. The elementary cross section of the $\gamma + p \rightarrow p + \omega$ process is evaluated to be $0.3\mu\text{b}/\text{sr}$ [12].

First of all we show the result of the ω mesic nucleus formation spectra with the optical potential $V_\omega^{(a)}$ given in Eq. (8). Shown in Fig. 10 are the calculated spectra of the (γ, p) reaction on the ^{12}C target with various incident energies for $E_\gamma = 1.5, 2.0, 2.7$ and 3.0 GeV. So far the formation rate was calculated for the ideal kinemat-

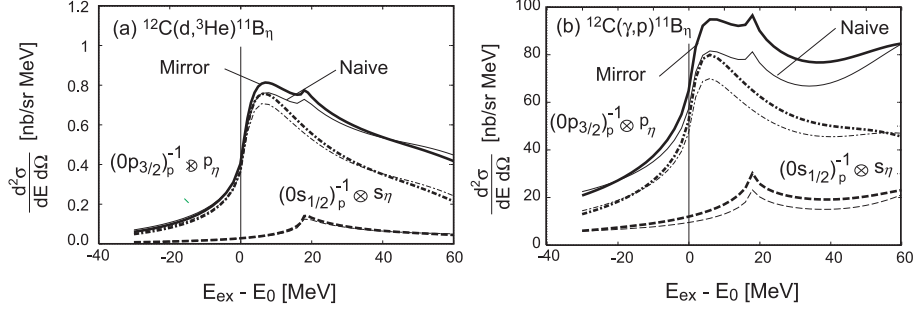


Figure 7: Calculated η -production spectra of the (a) $(d,^3\text{He})$ reaction at $T_d = 3.5$ GeV and (b) (γ,p) reaction at $E_\gamma = 950$ MeV for the ^{12}C target are shown as functions of the excitation energy E_{ex} defined in the text. E_0 is the η production threshold energy. The η -nucleus interaction are evaluated using the chiral doublet model with the mirror assignment (thick lines) and naive assignment (thin lines) with $C = 0.2$. The total spectra are shown by the solid lines and the dominant contributions from the $(0s_{1/2})_p^{-1} \otimes s_\eta$ and $(0p_{3/2})_p^{-1} \otimes p_\eta$ configurations are shown by the dashed lines and dash-dotted lines, respectively, where the proton-hole states are indicated as $(n\ell_j)_p^{-1}$ and η states as ℓ_η .

ics to satisfy the recoilless condition. Here we study also the photon energy dependence of the expected spectra and its subcomponent contributions so as to see the experimental feasibility in the lower energy photon facilities. The energy dependence of the expected spectra is also useful for the planned experiment at SPring-8 because it is required to use various photon energy around the ideal kinematics to have the data with better statistics [24]. As shown in Fig. 10, the spectra are dominated by the contributions from the two configurations $(0s_{1/2})_p^{-1} \otimes s_\omega$ and $(0p_{3/2})_p^{-1} \otimes p_\omega$ for the incident energies $E_\gamma = 2.7$ GeV and 3.0 GeV, which roughly satisfy the recoilless condition. Even in this ideal case for clear observations, the bound state structure is hardly seen in the spectra due to the large widths of the bound states. At $E_\gamma = 2.0$ GeV, the total spectrum is still dominated by the two configurations but other subcomponents have certain contributions above the ω production threshold. For $E_\gamma = 1.5$ GeV, we find that many configurations contribute to the total spectrum and, hence, it is not easy to extract the contributions of specific configurations any more.

It is worth pointing out here that the calculated results of the total spectra in Fig. 10 are similar for all cases shown here insensitively to the photon energy. Thus, we need to keep in mind that the contribution of each subcomponent has certain energy dependence even if the total spectrum has almost no energy dependence.

Next let us show the (γ, p) spectra calculated with the attractive potential $V_\omega^{(b)}$ and the repulsive potential $V_\omega^{(c)}$ defined in Eqs. (9) (10). We evaluate the spectra with these potentials at the incident photon energy $E_\gamma = 2.7$ GeV. As seen in Fig. 11(a), in the case of the attractive potential $V_\omega^{(b)}$, the bound state structure is clearly seen thanks to the narrow width of the bound state in p state and dominant contribution of the $(0p_{3/2})_p^{-1} \otimes p_\omega$ configuration. This is consistent with the (γ, p) spectrum shown in Ref. [12], in which the energy dependence on the ω optical potential is taken into account. Comparing these two spectra, we see that the energy dependence of the potential has relatively small contribution to fix the global shape of the spectra and the energy dependence affects on the reaction rate as a weak repulsion. In Fig. 11(b), we show the (γ, p) spectrum with the repulsive potential. Apparently the shape of the spectrum is quite different from the previous two attractive potentials. The repulsion of the omega meson inside the nucleus makes the spectrum push to higher energies and almost nothing is seen below the omega threshold. It would be interesting if one could measure the omega-nucleus system in the (γ, p) reaction around the threshold of the omega production.

Here we have obtained three types of plots for the formation spectra of the omega-nucleus system. In the first case, the optical potential $V_\omega^{(a)}$ has enough attraction to form bound states of the ω meson in nucleus, but the widths of the bound states are enlarged due to the strong absorption. Thus the whole spectrum of the (γ, p) reaction dose not show distinct peak structure caused by the bound states even at the ideal recoilless kinematics, in which the $(0p_{3/2})_p^{-1} \otimes p_\omega$ configuration dominants the spectrum. In the second case, since the optical potential $V_\omega^{(b)}$ has more attraction and less absorption, a deeper bound state of omega in p wave is formed with a narrower width. This bound state is clearly seen in the spectrum at the recoilless condition. In the third case, the optical potential $V_\omega^{(c)}$ is repulsive. The spectrum obtained with this potential has definitely different from the above two cases. The missing mass spectroscopy of the (γ, p) reaction in the omega pro-

duction energies is a good practical tool for the investigation of the omega-nucleus interaction, at least it will be clearly seen if the optical potential is attractive or repulsive.

4.3 σ -nucleus system

We propose the (γ, p) reaction as a new method to create the sigma meson inside a nucleus, as discussed in Ref. [18] with the $(d, {}^3\text{He})$ reaction. In this subsection, we discuss the sigma meson production in the (γ, p) reaction on a heavy nucleus target ${}^{208}\text{Pb}$. We show here the total spectral function formulated in Sec. 3.2 instead of the differential cross section because of lack of our knowledge for the elementary cross section of the sigma meson photoproduction. Since the total spectral function involves the effective number which counts the reaction rate of the picked-up proton induced by photon, we can investigate an impact of the narrow bound states of the sigma meson around the two pion threshold, showing the global shape of the spectral function without a definite number of the cross section. The incident photon energy in the (γ, p) reaction is chosen to be 400 MeV so as to satisfy the recoilless condition for two-pion production, since we are interested in the deeply bound sigma meson.

First of all, we show the total spectral functions $\rho_{\text{tot}}^{(d, {}^3\text{He})}(\omega)$ for the $(d, {}^3\text{He})$ reactions with the ${}^{208}\text{Pb}$ target for comparison. The incident deuteron energy is chosen to be 1.5 GeV in order to satisfy the recoilless condition around the emitted particle energy $T_f = T_i - 2m_\pi$. Figure 12(a) shows the plots of $\rho_{\text{tot}}^{(d, {}^3\text{He})}(\omega)$ for the $C = 0.2$ and 0.4 cases. In the $(d, {}^3\text{He})$ reaction, one finds a less prominent peak around $T_i - T_f = 2m_\pi$ for $C = 0.4$ as reported in Ref. [18]. It would be hard, however, to distinguish such a small peak in experiment. One sees also that the whole shape of the spectral function for $C = 0.4$ resembles that for $C = 0.2$. This is because the large distortion effect of the hadronic probe suppresses strongly production of the deeply bound states, which have the significant enhancement around $\omega \sim 2m_\pi$, and, hence, the total spectral function is dominated by the shallow bound states with large widths like the $C = 0.2$ case.

Next, in Fig. 12(b), we show the total spectral functions for the (γ, p) reaction on the ${}^{208}\text{Pb}$ target with $C = 0.2, 0.3$ and 0.4 as a function of the missing mass $T_i - T_f$. As shown in the figure, the spectral function of the $C = 0.4$ case is significantly enhanced around

$2m_\pi$ in a reflection of production of the deeply bound states thanks to the transparency of the (γ, p) reaction. The incident photon can go into the center of the nucleus, knocking out a proton lying in a deep state, and, as a consequence, the deeply bound sigma states with narrow widths are formed in the nucleus. This is the good advantage of the photon induced reaction. The figure shows also a peak structure of the spectral function with $C = 0.3$ above the two-pion threshold. This is also the consequence of production of the deeply bound sigma states.

In order to compare the energy dependence of the total spectral functions for the different strength of the chiral restoration, which is parameterized as C , we show in Fig. 12(c) spectral functions normalized so as to have the almost same peak height as the $C = 0.4$ case. The normalization factors are 10 for $C = 0.3$, 40 for $C = 0.2$ and 120 for $C = 0.0$. For comparison, we show also a spectral function with $C = 0.0$, in which the partial restoration of chiral symmetry does not take place. The spectral function with $C = 0.0$ is obtained in Ref. [27], having the peak around $T_i - T_f \simeq 550$ MeV. Note that the spectral function with $C = 0.0$ is calculated without the effective number and, therefore, the reaction mechanism is not involved in the spectral function unlike the cases of $C \neq 0.0$. Nevertheless the comparison gives us a schematic view of the energy dependence.

We can see the clear shift of the peak energy in this figure and can expect that the shift could be a good signal of the chiral restoration in the nuclear medium.

4.4 Background Consideration

So far we discuss the production rate of the mesons in nucleus in the (γ, p) reaction. In the missing mass spectroscopy of the emitting proton, the production of the meson in the nucleus is expected to be seen on top of a certain structureless background. In this section, we roughly estimate the background of the (γ, p) reactions.

First of all, in the η -nuclear system, the typical signal for the creation of the eta meson in nucleus is estimated to be 100 nb/(sr MeV) for the differential cross section of the $^{12}\text{C}(\gamma, p)$ reaction at the recoilless energy $E_\gamma = 950$ MeV as discussed in Sec. 4.1. On the other hand, experimental data [51] showed that the differential cross section of the inclusive $^{12}\text{C}(\gamma, p)$ reaction is $d^2\sigma/d\Omega dp \lesssim 0.9$ [$\mu\text{b}/(\text{sr MeV}/c)$]

at the photon energy $E_\gamma = 580$ MeV and the emitted photon angle $\theta_p = 23^\circ$ in the laboratory frame. From the data, we estimate the physical background due to the inclusive proton emission is

$$\frac{d^2\sigma}{d\Omega dE} = \frac{E}{p} \frac{d^2\sigma}{d\Omega dp} \sim 1.5 \left[\frac{\mu\text{b}}{\text{sr MeV}} \right] \quad (27)$$

in the proton energy distribution. Therefore, the signal over noise ratio is expected to be around 1/15. However, the kinematical condition of the (γ, p) reaction in Ref. [51] is different from that of the η -nucleus system formation reaction in Section 4.1. Hence, we need to use theoretical models and/or more appropriate experimental data to improve the background estimation.

As for the ω mesic nuclei formation by the (γ, p) reaction, the signal is estimated to be 10 nb/(sr MeV) for the ^{12}C target case in Sec.4.2, while the background is expected to be smaller than 100 nb/sr/MeV [24]. Thus, the signal over noise ratio is to be around 1/10 from the calculated results.

For the σ -nucleus systems, we do not have any background estimations so far, since we cannot evaluate definite values for the σ meson production rates due to lack of the elementary cross section. Conceivable physical backgrounds would be resonant enhancements of the cross section due to nucleon excitations in nucleus. Especially the kinematics considered here of the two pion production could conflict with a Δ excitation in nucleus. A possible way to avoid such a physical background is to observe more particles in the final state, for instance, with taking coincidence of the emitted proton and two pion with isospin 0. Another possibility might be to observe the (γ, p) reactions with lighter nuclear targets and to see the mass dependence of the peak around the two-pion threshold, since the deeply bound sigma states will not be seen in a lighter nucleus. The detailed discussions of the physical backgrounds are beyond the scope of the present paper.

5 Conclusion

In this paper we have made a theoretical evaluation of the formation rates of the η and ω mesons in nuclei induced by the (γ, p) reactions in ideal recoilless kinematics. We have shown the expected spectra in order to investigate the meson-nucleus interactions. We have found

that the (γ, p) reactions are good practical tool to investigate the properties of the mesons created deeply inside the nucleus due to the small distortion effects. This good advantage provides the distinct difference in the formation spectra of the η -nucleus system obtained by the two chiral models which are based on the different physical pictures of the $N(1535)$ resonance. For the ω -nucleus system, we have compared three types of the ω optical potentials in the (γ, p) spectra, showing the definitely different shapes of the spectra.

We have also investigate the (γ, p) spectra at the recoilless condition for the two pion production in isoscalar channel in order to study an impact of the creation of the deeply bound states of the sigma meson associated with the partial restoration of chiral symmetry in heavy nuclei. We have found that a prominent enhancement around the two pion threshold in the missing mass spectra in case of a sufficient strength of the partial restoration in medium, owing to the transparency of the (γ, p) reaction to create deeply bound states. Thus we expect that the (γ, p) reaction is a good tool to create the sigma meson in nucleus.

The study of the bound states is one of the most promising method to investigate the meson properties at finite density. Nevertheless the large natural widths of the meson bound states in nucleus disable to distinguish contributions from each bound state. In such a case, global conformation of the missing mass spectra is necessary to extract valuable information of the meson nucleus interaction. It is also beneficial to compare the spectra of the (γ, p) and $(d, {}^3\text{He})$ reactions at corresponding recoilless conditions, since each configuration differently contributes to the total spectra due to the different distortion effects. We expect that the present results stimulate the experimental activities and help the developments of this research field.

Acknowledgements

We would like to thank T. Hatsuda and T. Kunihiro for fruitful discussions on σ meson properties in nuclear medium. We acknowledge valuable discussions on photon induced reaction with N. Muramatsu and H. Yamazaki. We are also most grateful to M. Lutz for useful discussion on the ω - N scattering amplitude. We also thank E. Oset for his careful reading of our preprint and useful comments. This work

is partly supported by Grants-in-Aid for Scientific Research of Monbukagakusho and Japan Society for the Promotion of Science (No. 16540254). D.J. acknowledges support for his research work in Germany through a Research Fellowship of the Alexander von Humboldt Foundation.

References

- [1] For example; C.J. Batty, E. Friedman and A. Gal, Phys. Rep. **287**, 385 (1997).
- [2] H. Toki, S. Hirenzaki, T. Yamazaki, Nucl. Phys. **A530**, 679 (1991), S. Hirenzaki, H. Toki, T. Yamazaki, Phys. Rev. **C44**, 2472 (1991).
- [3] H. Gilg *et al.*, Phys. Rev. C **62**, 025201 (2000); K. Itahashi, *et al.*, *ibid.* **62**, 025202 (2000).
- [4] H. Geissel *et al.*, Phys. Rev. Lett. **88**, 122301 (2002).
- [5] P. Kienle, and T. Yamazaki, Phys. Lett. B **514**, 1 (2001); H. Geissel, *et al.*, *ibid.* **549**, 64 (2002); K. Suzuki, *et al.*, Phys. Rev. Lett. **92**, 072302 (2004).
- [6] D. Jido, H. Nagahiro and S. Hirenzaki, Phys. Rev. **C66**, 045202 (2002), Nucl. Phys. **A721**, 665c(2003).
- [7] H. Nagahiro, D. Jido and S. Hirenzaki, Phys. Rev. **C68**, 035205 (2003).
- [8] K. Tsushima, D.H. Lu, A.W. Thomas, K. Saito, Phys. Lett. **B443**, 26 (1998), K. Tsushima, D.H. Lu, A.W. Thomas, Phys. Rev. **C59**,1203 (1999).
- [9] R.S. Hayano, S. Hirenzaki, A. Gillitzer, Eur. Phys. J. A **6**, 99-105(1999).
- [10] M. Kohno and H. Tanabe, Phys. Lett. **B** 231(1989) 219-223.
- [11] A.I. Lebedev, V.A. Tryasuchev, J. Phys. G17, 1197 (1991).
- [12] E. Marco, W. Weise, Phys. Lett. **B** 502(2001) 59-62.
- [13] S. Hirenzaki, E. Oset, Phys. Lett. B **527**, 69 (2002).
- [14] See the reviews, T. Hatsuda and T. Kunihiro. Phys. Rep. **247**, 221 (1994); G.E. Brown and M. Rho, *ibid.* **269**, 333 (1996).

- [15] C. Garcia-Recio, J. Nieves, T. Inoue and E. Oset, Phys. Lett. **B550**, 47-54 (2002); T. Inoue and E. Oset, Nucl. Phys. **A710**, 354-370 (2002).
- [16] F. Klingl, N. Kaiser, W. Weise, Nucl. Phys. **A624**, 527 (1997).
- [17] F. Klingl, T. Waas, W. Weise, Nucl. Phys. **A650**, 299 (1999).
- [18] S. Hirenzaki, H. Nagahiro, T. Hatsuda, T. Kunihiro, Nucl. Phys. **A710**, 131-144(2002).
- [19] E.E. Kolomeitsev, N. Kaiser, and W. Weise, Phys. Rev. Lett. **90**, 092501 (2003).
- [20] S. Hirenzaki, Y. Okumura, H. Toki, E. Oset, and A. Ramos, Phys. Rev. C **61**, 055205 (2000).
- [21] O. Morimatsu, K. Yazaki, Nucl. Phys. **A435**, 727(1985); **A483**, 493(1988).
- [22] D. Trnka *et al.*, for the CBELSA/TAPS Collaboration, arXiv:nucl-ex/0504010.
- [23] M. Naruki *et al.*, arXiv:nucl-ex/0504016.
- [24] N. Muramatsu, private communication.
- [25] M. F. M. Lutz, G. Wolf and B. Friman, Nucl. Phys. A **706** (2002) 431
- [26] S. Chiku, T. Hatsuda, Phys. Rev. **D57**, R6 (1998),
S. Chiku, T. Hatsuda, Phys. Rev. **D58**, 076001 (1998),
M.K. Volkov, E.A. Kuraev, D. Blaschke, G. Ropke, S.M. Schmidt,
Phys. Lett. **B424**, 235(1998).
- [27] T. Hatsuda, T. Kunihiro, H. Shimizu, Phys. Rev. Lett. **82**, 2840 (1999).
- [28] D. Jido, T. Hatsuda, T. Kunihiro, Phys. Rev. **D63**, 011901(R) (2000).
- [29] Y. K. Kwon and F. Tabakin, Phys. Rev. C **18**, 932 (1978).
- [30] S. Hirenzaki, T. Kajino, K.-I. Kubo, H. Toki, I. Tanihata, Phys. Lett. B **194**, 20 (1987).
- [31] Q. Haider and L.C. Liu, Phys. Lett. B **172**, 257 (1986); Phys. Rev. C **34**, 1845(1986).
- [32] H. C. Chiang, E. Oset, and L. C. Liu, Phys. Rev. C **44**, 738 (1991).

- [33] R.E. Chrien *et al.*, Phys. Rev. Lett. **60**, 2595 (1988).
- [34] G.A. Sokol *et al.*, Fizika B8, 85 (1999).
- [35] M. Pfeiffer *et al.*, Phys. Rev. Lett. **92**, 252001 (2004).
- [36] C. DeTar and T. Kunihiro. Phys. Rev. D**39**, 2805 (1989).
- [37] D. Jido, M. Oka, and A. Hosaka, Prog. Theor. Phys. **106**, 873 (2001); D. Jido, Y. Nemoto, M. Oka, and A. Hosaka, Nucl. Phys. **A671**, 471 (2000).
- [38] Y. Nemoto, D. Jido, M. Oka, and A. Hosaka, Phys. Rev. **D57**, 4124(1998).
- [39] N. Kaiser, T. Waas, W. Weise, Nucl. Phys. **A612**, 297(1997).
- [40] T. Inoue, E. Oset, and M.J. Vicente Vacas, Phys. Rev. **C65**, 035204(2002).
- [41] M. Arima, K. Shimizu, and K. Yazaki, Nucl. Phys. **A543**, 613 (1992).
- [42] A.M. Green and S. Wycech, Phys. Rev. C **71**, 014001 (2005).
- [43] T. Hatsuda and M. Prakash, Phys. Lett. B **224**, 11 (1989).
- [44] H. Kim, D. Jido, and M. Oka, Nucl. Phys. **A640**, 77 (1998).
- [45] N. Kaiser, P.B. Siegel, W. Weise, Phys. Lett. **B362**, 23 (1995).
- [46] Y. Umemoto, S. Hirenzaki, K. Kume, H. Toki, Prog. Theor. Phys. **103**, 337 (2000); Phys. Rev. **C62**, 024606 (2000).
- [47] Review of Particle Physics, Particle Data Group; Phys. Lett. **B592**, 1, (2004).
- [48] S. Homma *et al.*, J. Phys. Soc. Jpn. **57**, 828 (1988).
- [49] S.L.Belostotskii et al., Sov.J.Nucl.Phys.41(6) 903 (1985).
- [50] K. Nakamura, S. Hiramatsu, T. Kamae, and H. Muramatsu, Phys. Rev. Lett. **33**, 853 (1974).
- [51] K. Baba *et al.*, Nucl. Phys. **A415**, 462 (1984).

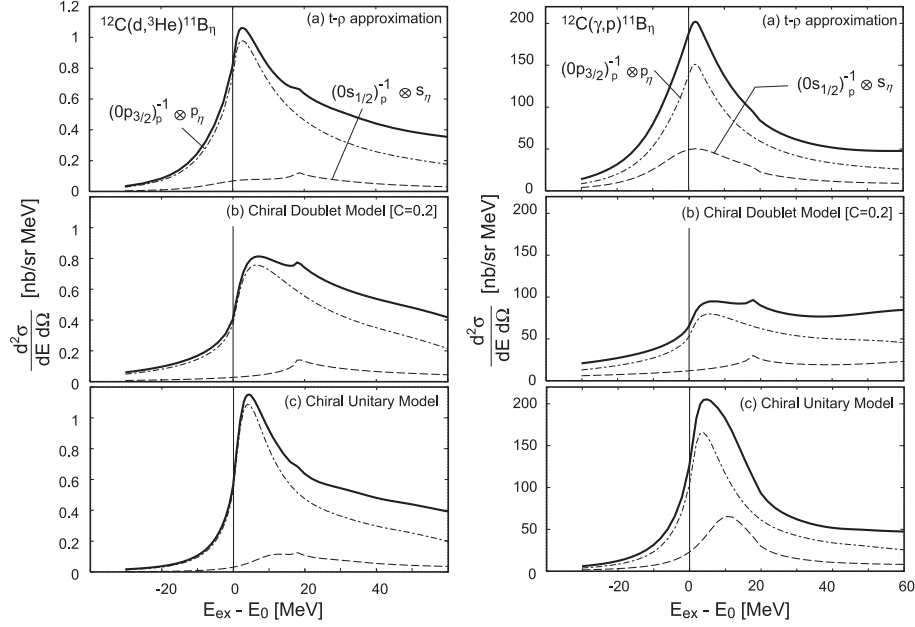


Figure 8: Calculated spectra of $^{12}\text{C}(d,^3\text{He})^{11}\text{B}\otimes\eta$ reactions at $T_d = 3.5$ GeV in the left-side and $^{12}\text{C}(\gamma,p)^{11}\text{B}\otimes\eta$ reactions at $E_\gamma = 950$ MeV in the right-side are shown as functions of the excitation energy E_{ex} defined in the text. E_0 is the η production threshold energy. The η -nucleus interactions are evaluated by (a) the t - ρ approximation, (b) the chiral doublet model with $C = 0.2$ and (c) the chiral unitary model [15]. The total spectra are shown by the thick solid lines, and the contributions from the dominant configurations $(0s_{1/2})_p^{-1} \otimes s_\eta$ and $(0p_{3/2})_p^{-1} \otimes p_\eta$ are shown by dashed lines and dash-dotted lines, respectively, where the proton-hole states are indicated as $(n\ell_j)_p^{-1}$ and the η states as ℓ_η .

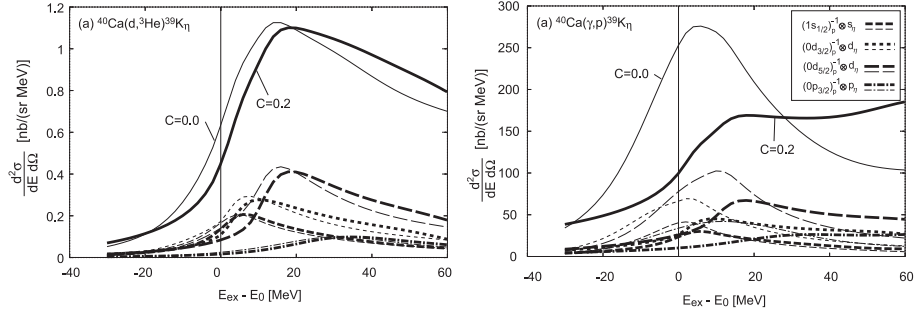


Figure 9: Calculated spectra for the formation of the η -mesic nuclei in (a) the $(d, {}^3\text{He})$ reaction at $T_d = 3.5$ GeV and (b) the (γ, p) reaction at $E_\gamma = 950$ MeV are shown as functions of the excitation energy E_{ex} defined in the text. E_0 is the η production threshold energy. The η -nucleus interaction are evaluated by the chiral doublet model with $C = 0.0$ and $C = 0.2$, and the expected spectra are shown by thin lines and thick lines, respectively. The total spectra are shown by the solid lines and dominant subcomponents are shown by dashed lines as indicated in the figures. Here, the proton-hole states are indicated as $(nl_j)_p^{-1}$ and the η states as l_η .

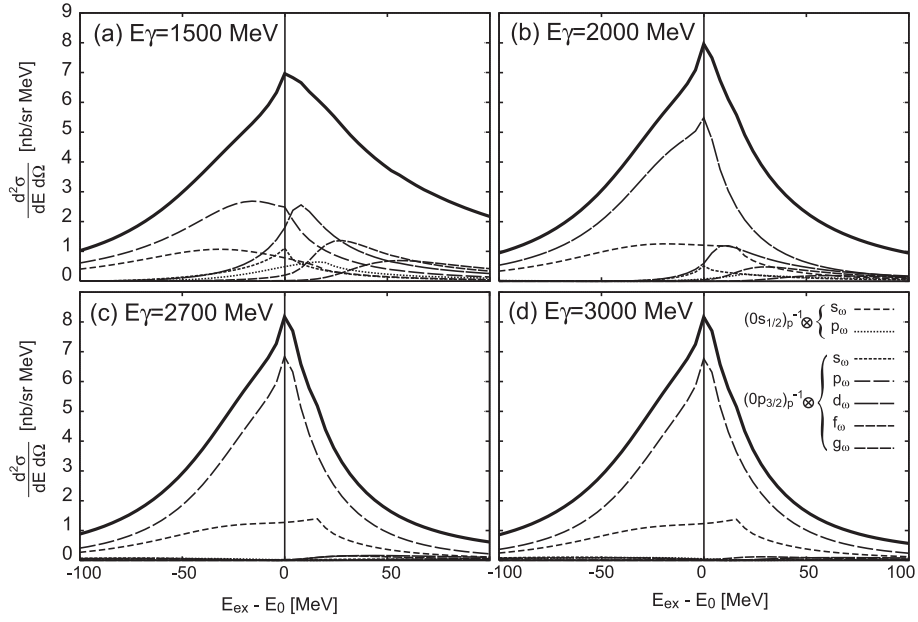


Figure 10: Calculated spectra of $^{12}\text{C}(\gamma, p)$ reaction for the formation of the ω - ^{11}B system with the attractive potential $V_{\omega}^{(a)}$ at (a) $E_{\gamma} = 1500$ MeV, (b) $E_{\gamma} = 2000$ MeV, (c) $E_{\gamma} = 2700$ MeV and (d) $E_{\gamma} = 3000$ MeV as functions of the excitation energy E_{ex} defined in the text. E_0 is the ω production threshold energy. The thick solid lines represent the total spectra and the other lines represent the contributions from the dominant subcomponents as indicated in the figures.

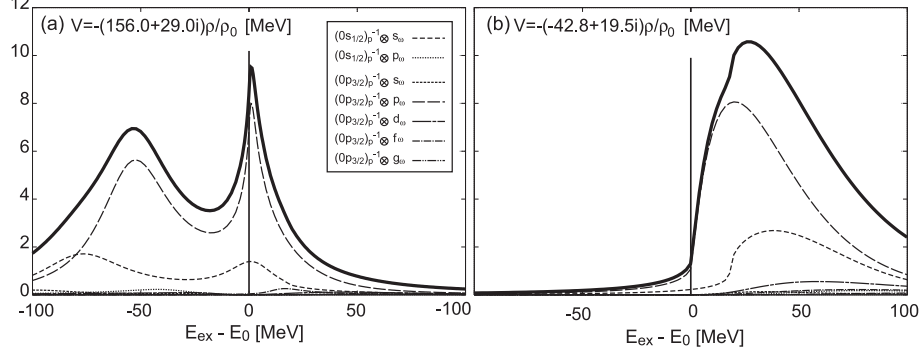


Figure 11: Formation spectra of the ω mesic nucleus in the (γ, p) reaction with the ^{12}C target calculated with the attractive potential $V_\omega^{(a)}$ (a) and the repulsive potential $V_\omega^{(b)}$ (b) at the photon energy $E_\gamma = 2.7$ GeV. E_0 is the ω production threshold energy. The thick solid lines represent the total spectra and the other lines represent the contributions from the dominant subcomponents as indicated in the figures.

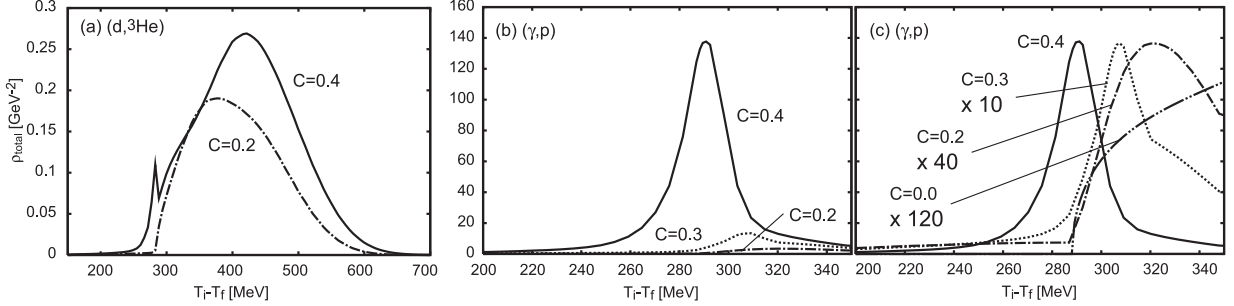


Figure 12: Total spectral functions ρ_{tot} defined in the text for (a) $(d, ^3\text{He})$ reactions and (b) (γ, p) reactions on ^{208}Pb target. The incident particle energies T_i are (a) 1.5 GeV and (b) 400 MeV, respectively. The solid lines indicate the spectral functions with the parameter $C = 0.4$. The dashed and the dash-dotted lines represent the spectral functions with $C = 0.3$ and $C = 0.2$, respectively. (c) Normalized spectral functions of the (γ, p) reactions. The normalization factors are 10, 40, 120 for the $C = 0.3$, $C = 0.2$ and $C = 0.0$ cases, respectively. The spectral function with $C = 0.0$ reported Ref. [27] is also shown for comparison.